Since January 2020 Elsevier has created a COVID-19 resource centre with free information in English and Mandarin on the novel coronavirus COVID-19. The COVID-19 resource centre is hosted on Elsevier Connect, the company's public news and information website.

Microchemical Journal 168 (2021) 106445

Contents lists available at ScienceDirect

Microchemical Journal

journal homepage: www.elsevier.com/locate/microc

Electrochemical immunosensor platform based on gold-clusters, cysteamine and glutaraldehyde modified electrode for diagnosing COVID-19

Lokman Liv

Electrochemistry Laboratory, Chemistry Group, The Scientific and Technological Research Council of Turkey, National Metrology Institute, (TUBITAK UME), Gebze, Kocaeli 41470 Turkey

ARTICLE INFO

Keywords:
Immunosensor
SARS-CoV-2
COVID-19
Gold-cluster
Square wave voltammetry

ABSTRACT

Amid the global threat caused by the coronavirus disease 2019 (COVID-19) pandemic, developing sufficiently rapid, accurate, sensitive and selective methods of diagnosing both symptomatic and asymptomatic cases is essential to alleviating and controlling the pandemic's effects. This article describes an electrochemical immunoassay platform developed to determine the severe acute respiratory syndrome-coronavirus-2 (SARS-CoV-2) spike antibody by using gold-clusters capped with cysteamine, glutaraldehyde, the spike protein of the SARS-CoV-2 antigen and bovine serum albumin on a glassy carbon electrode. The electrochemical oxidation signal of the antigen-based immunosensor at 0.9 V was used to detect the SARS-CoV-2 spike antibody. When saliva and oropharyngeal swab samples were analysed, the recovery and relative standard deviation values were 96.97%–101.99% and 4.99%–5.74%, respectively. The method's limit of detection relative to the SARS-CoV-2 spike antibody in synthetic media and in saliva or oropharyngeal swab samples was 0.01 ag/mL, while the immunosensor's linear response to the SARS-CoV-2 spike antibody varied from 0.1 to 1000 ag/mL. The cross-reactivity of the Middle East respiratory syndrome-coronavirus spike antigen was evaluated after being immobilised onto the functionalised gold-cluster based sensor, indicated that the good specifity of the produced immunosensor.

1. Introduction

After emerging from Wuhan in China's Hubei Province, the coronavirus disease 2019 (COVID-19), beginning as severe acute respiratory syndrome-coronavirus-2 (SARS-CoV-2), rapidly spread to more than 100 countries. SARS-CoV-2, a member of the genus *Betacoronavirus*, has oval structure and a size ranging from 60 nm to 140 nm [1]. As of 23 February 2021, more than 110 million cumulative cases of COVID-19 and 2.4 million deaths had been reported worldwide [2]. Because the course of COVID-19 can be asymptomatic, moderately flu-like or severe [3], the asymptomatic version, accounting for 20%–40% of cases, remains primarily responsible for its spread and the underestimation of cases, both of which continue to make the pandemic difficult to control [4–6]. Therefore, the early diagnosis of COVID-19 can be critical to determining whether to apply treatment. For that reason, simple, fast, accurate and highly sensitive methods of determining the SARS-CoV-2 antigen and antibody are urgently needed.

Many methods of diagnosing COVID-19 have been reported, including ones based on real-time polymerase chain reaction (RT-PCR) [7–14], lateral flow assay (LFA) [15], lateral flow immunoassay (LFIA) [1,16–19] enzyme-linked immunosorbent assay (ELISA) [20], plasmonic sensors [21,22] computed tomography (CT) imaging [23] and electrochemical biosensing technologies [3,24–31]. Despite being the primary and most sensitive and selective method of diagnosing COVID-19, RT-PCR is time-consuming and expensive, requires qualified personnel and can be run only in laboratory-based medical institutions [3,8,25,26]. Worse still, RT-PCR has demonstrated a high post-exposure false-negative ratio ranging from 20% to 67% [32,33] possibly caused by sampling, the source and quality of samples, and the poor sensitivity of diagnosing kits. These are also the common drawbacks of all the COVID-19 diagnostic tests. Of the six commercial diagnosing kits for COVID-19 reported to have high limits of detection (LOD) and result in false-negative results [34], ELISA-, LFA- and LFIA-based methods afford important benefits, including being inexpensive, easy to implement and moderately fast, despite having relatively low sensitivity that indicate false-negative results. Meanwhile, plasmonic sensor-based methods [21,22] are sensitive and inexpensive but entail complex experimental procedures and require highly experienced personnel, while CT imaging

E-mail address: lokman.liv@tubitak.gov.tr.

https://doi.org/10.1016/j.microc.2021.106445
Received 18 March 2021; Received in revised form 18 May 2021; Accepted 20 May 2021
Available online 24 May 2021

is not suitable for early diagnosis, quick response or on-site analysis [21,35].

By comparison, electrochemical methods of biosensing proteins, nucleic acids, bacteria, viruses, antibodies and their fragments have become attractive [36–40] in terms of some features such as simplicity, low cost, rapidity, robustness, high sensitivity and selectivity [40]. Owing to those advantages, electrochemical biosensors and methods have been developed to determine molecular SARS-CoV-2 antigens, antibodies, and/or their fragments. Among them, antigen-based methods rely on either molecular (e.g. viral RNA) [3,28] or viral proteins that are spike [25,27,29,30] or nucleocapsid [26,31]. In the former, for the best LOD (i.e. 200 copies/mL in clinical specimen, 3 aM ORF1ab gene in synthetic media) and dynamic response (10^{-17}–10^{-12} M ORF1ab gene), preparing the electrochemical sensor and performing the measurement takes 29 h and 3 h, respectively [28]. In the latter [25,27,29,30], despite a brief period of measurement except the method developed by Mojsoska et al. [30] with a measurement step of about 45 min, preparing the sensors can take between 5 h and 12 h. Rahmati et al. [29] have obtained a LOD of 0.04 fg/mL in synthetic media, while Seo et al. [25] have achieved LODs of 1 fg/mL in synthetic media and 100 fg/mL in clinical specimens. On the contrary, Vadlamani et al. [27] and Mojsoska et al. [30] have obtained LODs at the high magnitudes of μg/mL in synthetic and plaque assay media, respectively. The methods involving nucleocapsid proteins, preparing the electrochemical sensor takes 25 h [31] and less than 2 h [26]. The first method could detect 0.8 pg/mL of nucleocapsid protein in 30 min in synthetic media [31]. The second method, which also includes immunosensor studies with the SARS-CoV-2 spike and nucleocapsid antibodies, has no information regarding the LOD and dynamic range [26]. In one such study, the researchers determined the SARS-CoV-2 spike or nucleocapsid antibodies in 30 min, but the LODs were at high levels in terms of ng/mL [24].

In view of those drawbacks, it was aimed to develop an immunoassay platform and voltammetric method of determining the SARS-CoV-2 spike antibody able to overcome the mentioned limitations. To that end, it was created a novel immunoassay platform involving gold (Au)-clusters capped with cysteamine (CysAm), glutaraldehyde (GluAl), the spike protein of the SARS-CoV-2 antigen (S-gene) and bovine serum albumin (BSA) on a glassy carbon electrode (GCE)–altogether, BSA/S-gene/GluAl/CysAm/Au/GCE–for a simple, rapid, low-cost, ultrasensitive way of voltammetrically determining the SARS-CoV-2 spike antibody in real as well as synthetic samples.

2. Experimental

2.1. Chemicals and equipment

The SARS-CoV-2 (2019-nCoV) spike S1-his recombinant protein (verified by HPLC, Cat: 40591-V08H), SARS-CoV-2 spike antibody (Chimeric MAb Cat: 40150-D00) and Middle East respiratory syndrome-coronavirus (MERS-CoV) spike-S1 protein (S1 Subunit, aa 1–725, His Tag, Cat: 40069-V08B1) were purchased from Sino Biological Inc. Standard Au solution (1000 mg Au/ampoule ($HAuCl_4{\cdot}3H_2O$ in 12.7% HCl), Merck 109868), cysteamine hydrochloride (BioXtra, Sigma 30078), glutaraldehyde (50% in water, Merck 814393), bovine serum albumin (≥98, Sigma-Aldrich 05470), phosphate buffered saline (PBS, tablet, Sigma-Aldrich P4417, 0.01 M phosphate buffer, 0.0027 M potassium chloride and 0.137 M sodium chloride, pH 7.4, at 25 °C) and all other chemicals were of analytical reagent grade.

All solutions with the antibody and antigen were prepared in 0.01 M PBS solution and stored in Eppendorf protein LoBind tubes, whereas all other solutions (only GluAl was in dimethyl formamide), were prepared in ultrapure water and stored in high-density polyethylene falcon tubes. Milli-Q Direct 8 system was used to produce ultrapure water.

A Metrohm Autolab PGSTAT 128N potentiostat-galvanostat consisting of chemically modified glassy carbon electrode (Au-clusters capped with CysAm, GluAl, S-gene and BSA modified GCE–BSA/S-gene/GluAl/CysAm/Au/GCE, supporting material: BASi MF-2012 GCE) as the working electrode, Ag/AgCl/3 M NaCl (BASi MF-2052 RE-5B) as a reference electrode and platinum wire (BASi MW-1032, 7.5 cm) as an auxiliary electrode for the voltammetric determination of the SARS-CoV-2 spike antibody in synthetic and real samples.

A Mettler Toledo Seven Excellence pH meter with InLab Routine Pro-ISM combined pH electrode was used to measure pH, and a FEI Quanta FEG 250 environmental scanning electron microscope with FEI Quanta 250 XFLASH 5030 energy dispersive X-ray spectroscopy module was used to characterise the surfaces of the electrodes.

2.2. Preparation of the SARS-CoV-2 immunosensor

To prepare the BSA/S-gene/GluAl/CysAm/Au/GCE sensor, the surface of the GCE was lustered with 0.05 μm of alumina suspension on felt, followed by rinsing with ultrapure water. The GCE was subsequently exposed to ultrasonic waves in a 1:1 ethanol–ultrapure water mixture and in ultrapure water for 5 min each. The Au-clusters were formed on the electrode surface by using cyclic voltammetry for 20 cycles in a range of potential between 0.1 V and 0.9 V in 6 mM $HClO_4$ and 0.1 M HCl. After being washed with ultrapure water, 25 μL of 20 mM CysAm was dropped onto the electrode (i.e. Au/GCE) for 1 h, then thiol sites of the CysAm were chemisorbed on the surface of the Au/GCE. After another washing with ultrapure water, the electrode (i.e. CysAm/Au/GCE) was incubated for 1 h with 25 μL of 7.5% GluAl in dimethyl formamide. Next, the surface of the electrode (i.e. GluAl/CysAm/Au/GCE) was covered with 10 μL of S-gene, and incubated for 45 min. This reaction based on the imine formation of the aldehyde group in glutaraldehyde and the amine group in the S-gene in 0.01 M PBS solution (pH 7.5). Last, free spaces of the electrode (i.e. S-gene/GluAl/CysAm/Au/GCE) were blocked with 2% BSA for 20 min to produce BSA/S-gene/GluAl/CysAm/Au/GCE. All incubations were performed at room temperature, and upon completion, the sensor was stored at 4 °C until further use.

All steps for preparing the BSA/S-gene/GluAl/CysAm/Au/GCE sensor and measuring the SARS-CoV-2 spike antibody are illustrated in Fig. 1.

2.3. Measurement procedure

Once the sensor was prepared, the SARS-CoV-2 spike antibody was kept on the sensor for 30 min, and square wave voltammetry measurements were taken between 0.1 V and 1.4 V with 5 mV of step potential, 20 mV of pulse amplitude, 10 Hz of frequency and 0.1 s of interval time. Cyclic voltammetry measurements were taken in the same potential range with 2.5 mV of step amplitude and 50 mV/s of scan rate. The solution containing 0.01 M PBS solution (pH 7.5) and the appropriate amount of the SARS-CoV-2 spike antibody or real spiked sample with a final volume of 10 mL was used. The peak of the BSA/S-gene/GluAl/CysAm/Au/GCE sensor at 0.9 V decreased with the addition of the SARS-CoV-2 spike antibody, which was evaluated as a response for determining the SARS-CoV-2 spike antibody. The measurements were taken at 21 ± 3 °C and 45 ± 15% relative humidity.

2.4. Sample preparation

Saliva and oropharyngeal swab samples were collected from six healthy individuals and half of the samples were spiked with 20 ag/100 μL (1 ag/5 μL) of the SARS-CoV-2 spike antibody, then all of the samples were transferred into 1 mL of lysis buffer solution containing 50 mM Tris-Tris.HCl (pH 7.5), 1 mM dithiothreitol, 100 mM NaCl and 5% glycerol. Afterwards, 5 μL of the spiked and pretreated oropharyngeal swab and saliva samples were deposited onto the immunosensor platform and analysed using external calibration.

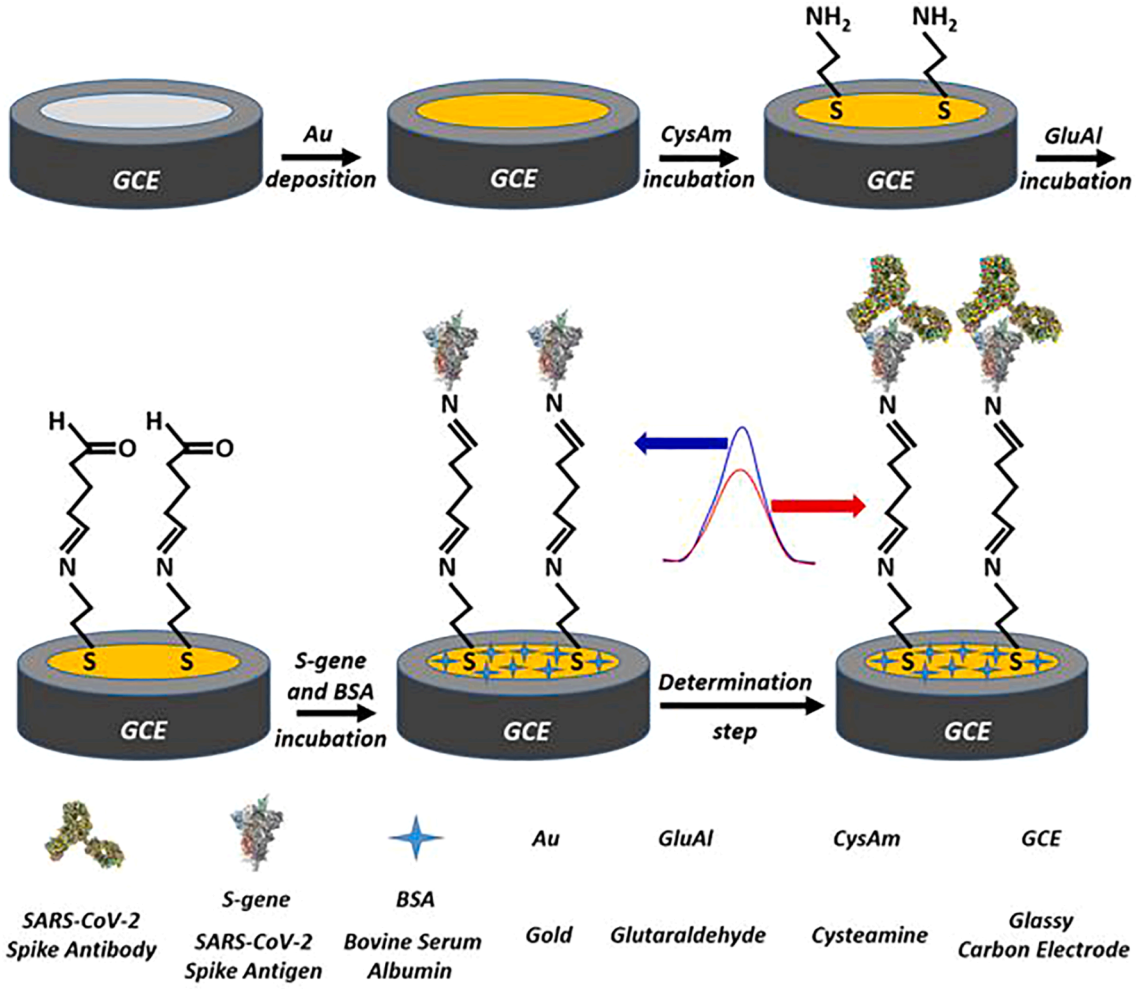

Fig. 1. Schematic presentation of the procedure of preparing the BSA/S-gene/GluAl/CysAm/Au/GCE and measuring the SARS-CoV-2 spike antibody.

3. Results and discussion

3.1. Sensor characterisation

Cyclic voltammetry (CV), scanning electron microscopy (SEM) and energy dispersive X-ray spectroscopy (EDX) techniques were used to characterise the surfaces of the electrodes after each modification and the results consistent with the literature were obtained [40]. In particular, cyclic voltammograms of the GCE, Au/GCE, CysAm/Au/GCE, GluAl/CysAm/Au/GCE, S-gene/GluAl/CysAm/Au/GCE and BSA/S-gene/GluAl/CysAm/Au/GCE electrodes in 2 mM of $K_3[Fe(CN)_6]$ appear in Fig. 2. After the Au-clusters were modified on the bare GCE, the peak heights of redox couple considerably increased owing to the enlarged surface area of the electrode and the improved rate of electron transfer (Fig. 2b). The peak heights of the redox couple also increased after the incubation of CysAm on the Au/GCE (Fig. 2c) due to the electrostatic interaction and attraction between the $[Fe(CN)_6]^{3-}$/$[Fe(CN)_6]^{4-}$ couple and the amine terminals of the CysAm/Au/GCE [40]. With GluAl and S-gene modified on the CysAm/Au/GCE, the peak heights decreased for each electrode (Fig. 2d, e), which it was attributed to the physical barriers of GluAl and S-gene hindering the redox couple from reaching the surface of the GluAl/CysAm/Au/GCE or S-gene/GluAl/CysAm/Au/GCE. Since the $[Fe(CN)_6]^{3-}$/$[Fe(CN)_6]^{4-}$ couple cannot approach the innermost of this electrode due to the physical barrier and BSA fills the empty surfaces of this innermost part, it is considered as usual for the current values not to be changed (Fig. 2f). In addition, when the experiments were carried out without BSA modification, it was observed that the peaks became flat, their intensities decreased and reproducible results were not obtained. Thus, BSA modification was also made while producing the sensor.

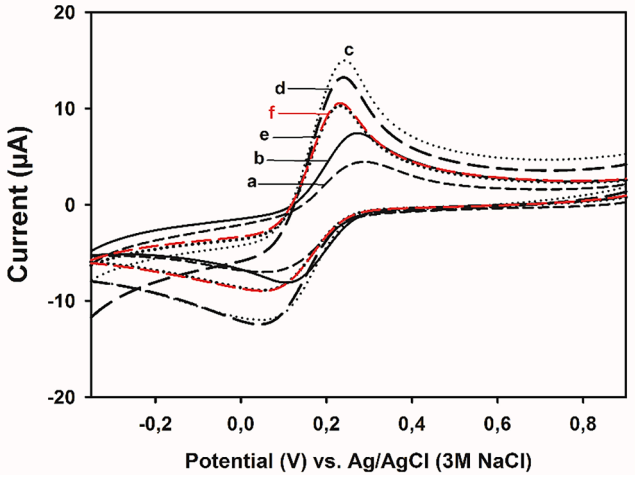

Fig. 2. Cyclic voltammograms of (a) GCE, (b) Au/GCE, (c) CysAm/Au/GCE, (d) GluAl/CysAm/Au/GCE, (e) S-gene/GluAl/CysAm/Au/GCE and (f) BSA/S-gene/GluAl/CysAm/Au/GCE in 2 mM $K_3[Fe(CN)_6]$ with a scan rate of 50 mV/s.

SEM images and EDX spectra for the bare GCE, Au/GCE, CysAm/Au/

GCE, GluAl/CysAm/Au/GCE and BSA/S-gene/GluAl/CysAm/Au/GCE appear in Figs. 3 and S1, respectively. As expected, a flat SEM image and an EDX spectrum containing only carbon and oxygen were obtained for the bare GCE (Figs. 3A and S1A). As shown in Fig. 3B, Au-clusters deposited onto the GCE's surface with a roundish shape, and the EDX spectrum (Fig. S1B) showed that more than half of the GCE's surface was covered by Au. The enlargement of the Au-clusters and the sharpness of the structures indicate that modification with CysAm on the Au/GCE's surface had occurred. Added to that, nitrogen peaks appeared in the EDX spectrum due to lingering nitrogen terminals on the surface when CysAm bound from the sulphur terminal to the Au-clusters (Fig. S1C). The sharp structures and particle size ratios continued to rise with the modification of GluAl on the CysAm/Au/GCE, and thready, cloudy structures emerged due to GluAl's long chain structure. Because GluAl attached to the surface at CysAm's amine terminals, the nitrogen content at the surface of the CysAm/Au/GCE dropped from 3% to 2.2% in the GluAl/CysAm/Au/GCE (Fig. S1D). Upon the immobilisation of the S-gene and BSA on the GluAl/CysAm/Au/GCE, the particle size ratios rose slightly, whereas the sharp and thready, cloudy structures decreased on the surface, likely due to the bulky structures of the S-gene and BSA as appear in Fig. 3E. Last, the amount of heteroatoms on the surface, especially the occurrence of sulphur and increasing of nitrogen, indicates that the protein-like structures attached to the surface (Fig. S1E).

All of the CV, SEM and EDX measurements confirmed that the electrode modifications were successfully performed for the voltammetric determination of the SARS-CoV-2 spike antibody in synthetic and real samples.

3.2. Cyclic voltammetric characteristics of the system

CV was used to clarify the electrode reaction mechanism belonging to the SARS-CoV-2 spike antibody by using the BSA/S-gene/GluAl/CysAm/Au/GCE. As shown in Fig. S2, the immunosensor in the supporting electrolyte solution had an oxidation peak at 0.9 V, which decreased as the SARS-CoV-2 spike antibody was added. The irreversibility of the electrode reaction could be associated with the repulsive forces formed between the partially negative species oxidizing at the electrode surface and the negative phosphate species ($H_2PO_4^-$ and HPO_4^{2-}) in the media, and thus the loss of the electron transfer. CV scans performed at increasing scan rates to determine whether the SARS-CoV-2 spike antibody's relocation to the sensor's surface was diffusion- or adsorption-controlled revealed plots of the peak height (I_p, μA) – scan rate (υ, V/s) and the peak height (I_p, μA) – the square root of the scan rate ($\sqrt{\upsilon}$, $\sqrt{\text{V/s}}$) of $I_p = 189.27\upsilon + 2.08 (R^2 = 0.996)$ and $I_p = 89.87\sqrt{\upsilon} - 7.93 (R^2 = 0.999)$, respectively (Fig. S3). The linearity of both equations showed that the system was based on a joint adsorption- and diffusion-controlled electrode reaction.

3.3. Optimisation studies

Parameters affecting the immunosensor's performance were investigated in the presence of 10 ag/mL of the SARS-CoV-2 spike antibody. As a result, the concentration of CysAm, GluAl and S-gene, and the binding time of CysAm, GluAl, S-gene, BSA and the SARS-CoV-2 spike antibody were respectively optimised to 20 mM, 7.5%, 5 μg/mL, 1 h, 1 h, 45 min, 20 min and 30 min, as shown in Fig. S4 for the voltammetric determination of the SARS-CoV-2 spike antibody in synthetic and real samples. Because the pH of body fluids usually remains in a roughly neutral range, measurements were performed in 0.01 M (pH 7.5) PBS solution.

3.4. Method validation

The groups containing heteroatoms such as hydroxyl on the surface of the SARS-CoV-2 spike antibody were oxidized during the anodic scan.

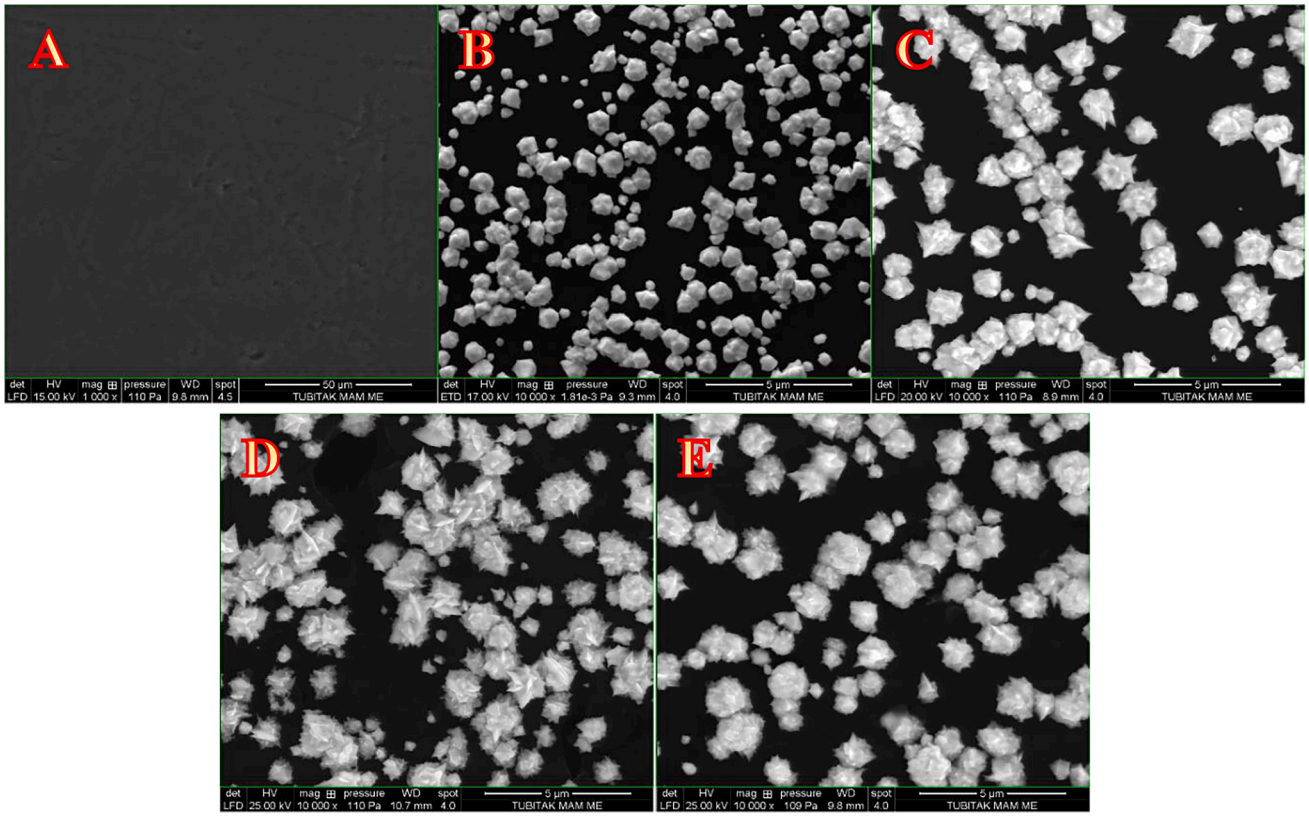

Fig. 3. SEM images for (A) bare GCE, (B) Au/GCE, (C) CysAm/Au/GCE, (D) GluAl/CysAm/Au/GCE and (E) BSA/S-gene/GluAl/CysAm/Au/GCE (SEM analysis: 20 kV voltage, 4.0 spot value, ETD detector).

The peak height of the developed sensor decreased in the presence of the SARS-CoV-2 spike antibody in 0.01 M (pH 7.5) PBS solution due to the large size of immuno-complex to block the electron transfer, which was compatible with the literature [38]. The square wave voltammograms and curve belonging to the SARS-CoV-2 spike antibody appear in Fig. 4. ΔI_p values were calculated by subtracting the new signal generated by the added SARS-CoV-2 spike antibody from the signal of the immunosensor. The LOD and analytical range for the SARS-CoV-2 spike antibody found while using the BSA/S-gene/GluAl/CysAm/Au/GCE were 0.01 ag/mL (i.e. from blank signal) and 0.1–1000 ag/mL in 0.01 M (pH 7.5) PBS solution.

The MERS-CoV spike antigen (M-S-gene) was immobilised on the GluAl/CysAm/Au/GCE and blocked with BSA, for BSA/M-S-gene/GluAl/CysAm/Au/GCE, to gauge the proposed method's selectivity. As a result, the fabricated sensor showed no response to 1 ag/mL of the SARS-CoV-2 spike antibody (Fig. S5). Moreover, the interference effects of some enzymes, compounds and ions that could be found in saliva were investigated in a solution containing 1 ag/mL of the SARS-CoV-2 spike antibody as shown in Table 1. A 5% variation in the peak height was employed as the criterion for the evaluation of tolerable amounts or ratios. The results showed that the developed method was not affected by the large amounts of interferences.

Since temperature is the most important parameter for the evaluation of method robustness and sensor stability/robustness in biosensor studies, it was extensively investigated. In the former, the method robustness was evaluated using the data in Fig. 4, since it included the changes in humidity difference (45 ± 15% relative humidity) in addition to temperature difference (21 ± 3 °C). RSD% values obtained between 5.01% and 7.36% for 10, 100 and 1000 ag/mL of the SARS-CoV-2 spike antibody in the respective temperature and humidity ranges show that the system is adequately robust. In the latter, the sensor stability was examined by measuring the peak height at the end of each 3 d for 30 d and it was observed that the signal received on the first day was preserved as 94.1% on the 30th day as shown in Fig. S6. As for the sensor robustness, it was investigated similar to the sensor stability study at 25 °C and 37 °C for 30 d as appear in Fig. S7 and it was found that the signal received on the first day was preserved as 91.4% and 80.0% at 25 °C and 37 °C on the 30th day, respectively. As a result, the sensor is a very stable and robust platform for the detection of the SARS-CoV-2 spike antibody despite the strict temperature conditions.

3.5. Sample application

When the developed method was applied to the spiked and pretreated saliva and oropharyngeal swab samples to determine the SARS-CoV-2 spike antibody, the relative standard deviation and recovery values varied from 4.99% to 5.74% and 96.97% to 101.99%, respectively. Voltammograms and results for the spiked saliva and oropharyngeal swab samples appear in Figs. S8, S9 and Table 2. The results generally suggest that the method offers good precision and trueness.

4. Conclusion

A rapid (~35 min), inexpensive (3 €/test), easy-to-use, ultrasensitive immunosensor platform is presented for voltammetrically determining the SARS-CoV-2 spike antibody in spiked saliva and oropharyngeal swab samples. The developed biosensor has a shorter preparation and similar analysis time compared to some prominent electrochemical methods in the literature [25,27–30]. In addition, the developed method is better than the RT-PCR technique in terms of analysis time and cost [7–14]. Beyond that, to the best of my knowledge, the sensor has achieved the best LOD of reported voltammetric immunoassays [24–27,29–31]. In the context of immunoassays described in the literature, the developed sensor also offers relative simplicity, ultrasensitivity and a wide analytical range. It was proposed that using saliva and oropharyngeal swab samples instead of time-consuming blood and serum samples requiring various processes, as well as avoiding the non-response of the SARS-CoV-2 spike antibody to the sensor produced based on MERS-CoV, may have allowed the platform's mentioned benefits. On top of that, the results of the spiked saliva and oropharyngeal swab samples revealed the proposed method's relative accuracy. Moving forward, the developed immunosensor could be readily integrated into a ready-to-use commercial kit.

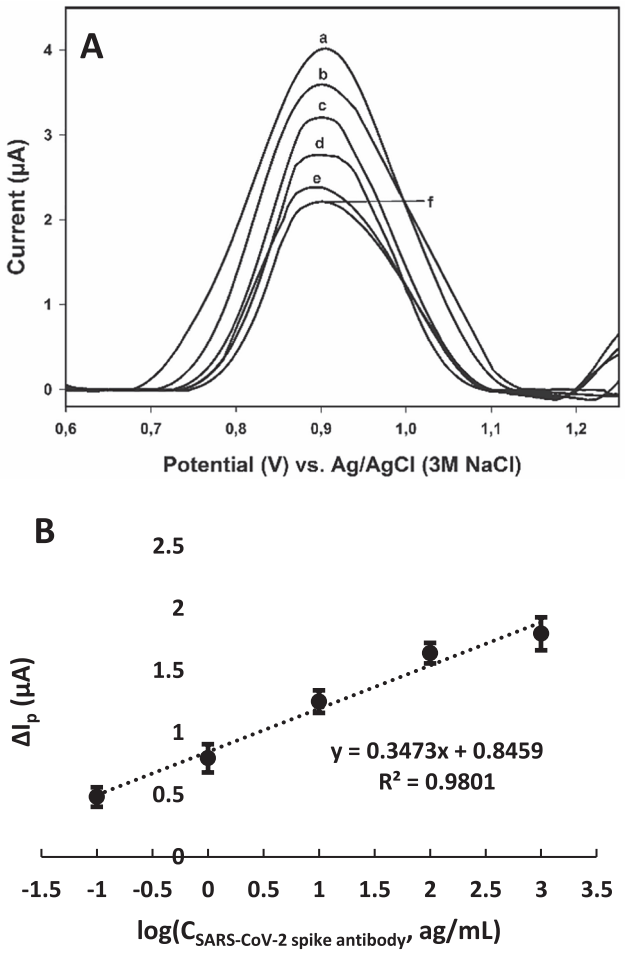

Fig. 4. (A) The square wave voltammograms and (B) the calibration curve (n = 3 for each concentration) at BSA/S-gene/GluAl/CysAm/Au/GCE in 0.01 M (pH 7.5) PBS solution. (a) 0.01 M (pH 7.5) PBS solution, (b) +0.1 ag/mL, (c) +1 ag/mL, (d) +10 ag/mL, (e) + 100 ag/mL and (f) +1000 ag/mL of the SARS-CoV-2 spike antibody.

Table 1
The results of interference studies for the detection of the SARS-CoV-2 spike antibody. Conditions: 1 ag/mL of the SARS-CoV-2 spike antibody, 0.01 M (pH 7.5) PBS solution.

Interference	Tolerable amount[a] (unit/mL)	Tolerable ratio[b]
α-Amylase	500	–
Lipase	100	–
Na^+, K^+	–	1000
Ca^{2+}, Mg^{2+}	–	500
$H_2PO_4^-$, HPO_4^{2-}	–	400
Urea	–	350
HCO_3^-	–	300
NH_3	–	250

[a] The tolerable amounts were calculated by performing measurements in PBS solution after the relevant enzymes were transferred to the lysis buffer.
[b] The tolerable ratios were calculated by direct measurement in PBS solution.

Table 2
The results of spiked saliva and oropharyngeal swab samples (n = 6).

Sample	Added amount of SARS-CoV-2 spike antibody (1 ag/5 μL)	SARS-CoV-2 spike antibody found (mean ± standard deviation; ag/5 μL)	Recovery (%) (mean ± standard deviation)	Relative standard deviation (%)
Saliva	1	1.020 ± 0.058	101.99 ± 5.85	5.74
Oropharyngeal swab	1	0.970 ± 0.048	96.97 ± 4.84	4.99

CRediT authorship contribution statement

Lokman Liv: Conceptualization, Methodology, Formal analysis, Investigation, Validation, Visualization, Writing - original draft, Writing - review & editing.

Declaration of Competing Interest

The authors declare that they have no known competing financial interests or personal relationships that could have appeared to influence the work reported in this paper.

Acknowledgements

This study was performed in the Electrochemistry Laboratory of TUBITAK UME. The authors would like to thank to Melisa Yener, Gizem Çoban and Şevval Arzu Can for some voltammetric measurements, and Sevgi Gülyüz at TUBITAK MAM-Materials Institute for SEM and EDX measurements.

Appendix A. Supplementary data

Supplementary data to this article can be found online at https://doi.org/10.1016/j.microc.2021.106445.

References

[1] D. Wang, S. He, X. Wang, Y. Yan, J. Liu, S. Wu, S. Liu, Y. Lei, M. Chen, L. Li, et al., Rapid lateral flow immunoassay for the fluorescence detection of SARS-CoV-2 RNA, Nat. Biomed. Eng. 4 (2020) 1150–1158.
[2] WHO, Weekly Epidemiological UPDATE – 23 February 2021. https://www.who.int/publications/m/item/weekly-epidemiological-update—23-february-2021, 2021 (accessed 16 March 2021).
[3] M. Alafeef, K. Dighe, P. Moitra, D. Pan, Rapid, ultrasensitive, and quantitative detection of SARS-CoV-2 using antisense oligonucleotides directed electrochemical biosensor chip, ACS Nano 14 (2020) 17028–17045.
[4] M. Kenji, K. Katsushi, Z. Alexander, C. Gerardo, Estimating the asymptomatic proportion of coronavirus disease 2019 (COVID-19) cases on board the Diamond Princess cruise ship, Yokohama, Japan, 2020, Euro Surveill 25 (2020) 2000180.
[5] H. Nishiura, T. Kobayashi, T. Miyama, A. Suzuki, S. Jung, K. Hayashi, R. Kinoshita, Y. Yang, B. Yuan, A.R. Akhmetzhanov, et al., Estimation of the asymptomatic ratio of novel coronavirus infections, Int. J. Infect. Dis. 94 (2020) 154–155.
[6] D.P. Oran, E.J. Topol, Prevalence of asymptomatic SARS-CoV-2 infection: a narrative review, Ann. Intern. Med. 173 (2020) 362–367.
[7] P. Yang, D. Zhang, P. Yang, L.L.M. Poon, Q. Wang, Viral load of SARS-CoV-2 in clinical samples, Lancet Infect. Dis. 20 (2020) 411–412.
[8] Y. Li, L. Yao, J. Li, L. Chen, Y. Song, Z. Cai, C. Yang, Stability issues of RT-PCR testing of SARS-CoV-2 for hospitalized patients clinically diagnosed with COVID-19, J. Med. Virol. 92 (2020) 903–908.
[9] J.F. Chan, C.C. Yip, K.K. To, T.H. Tang, S.C. Wong, K.H. Leung, A.Y. Fung, A.C. Ng, Z. Zou, H. Tsoi, et al., Improved molecular diagnosis of COVID-19 by the novel, highly sensitive and specific COVID-19-RdRp/Hel real-time reverse transcription-PCR assay validated in vitro and with clinical specimens, J. Clin. Microbiol. 58 (2020) e00310–e00320.
[10] L. Lan, D. Xu, G. Ye, C. Xia, S. Wang, Y. Li, H. Xu, Positive RT-PCR test results in patients recovered from COVID-19, JAMA 323 (2020) 1502–1503.
[11] S.W. Park, D.M. Cornforth, J. Dushoff, J.S. Weitz, The time scale of asymptomatic transmission affects estimates of epidemic potential in the COVID-19 outbreak, Epidemics 31 (2020) 1–18.
[12] P.B. Van Kasteren, B. van der Veer, S. van den Brink, L. Wijsman, J. de Jonge, A. van den Brandt, R. Molenkamp, C.B.E.M. Reusken, A. Meijer, Comparison of seven commercial RT-PCR diagnostic kits for COVID-19, J. Clin. Virol. 128 (2020), 104412.
[13] M. Yang, S. Chen, B. Huang, J.M. Zhong, H. Su, Y.J. Chen, Q. Cao, L. Ma, J. He, X. Li, et al., Pathological findings in the testes of COVID-19 patients: clinical implications, Eur. Urol. Focus 6 (2020) 1124–1129.
[14] B. Visseaux, Q. Le Hingrat, G. Collin, D. Bouzid, S. Lebourgeois, D. Le Pluart, L. Deconinck, F. Lescure, J. Lucet, L. Bouadma, et al., Evaluation of the QIAstat-Dx respiratory SARS-CoV-2 panel, the first rapid multiplex PCR commercial assay for SARS-CoV-2 detection, J. Clin. Microbiol. 58 (2020) e00630–e00720.
[15] J.P. Broughton, X. Deng, G. Yu, C.L. Fasching, V. Servellita, J. Singh, X. Miao, J. A. Streithorst, A. Granados, A. Sotomayor-Gonzalez, et al., CRISPR–Cas12-based detection of SARS-CoV-2, Nat. Biotechnol. 38 (2020) 870–874.
[16] B.G. Andryukov, Six decades of lateral flow immunoassay: from determining metabolic markers to diagnosing COVID-19, AIMS Microbiol. 6 (2020) 280–304.
[17] C. Huang, T. Wen, F.J. Shi, X.Y. Zeng, Y.J. Jiao, Rapid detection of IgM antibodies against the SARS-CoV-2 virus via colloidal gold nanoparticle-based lateral-flow assay, ACS Omega 5 (2020) 12550–12556.
[18] L. Zeng, Y. Li, J. Liu, L. Guo, Z. Wang, X. Xu, S. Song, C. Hao, L. Liu, M. Xin, et al., Rapid, ultrasensitive and highly specific biosensor for the diagnosis of SARS-CoV-2 in clinical blood samples, Mater. Chem. Front. 4 (2020) 2000–2005.
[19] Z. Chen, Z. Zhang, X. Zhai, Y. Li, L. Lin, H. Zhao, L. Bian, P. Li, L. Yu, Y. Wu, et al., Rapid and sensitive detection of anti-SARS-CoV-2 IgG using lanthanide-doped nanoparticles-based lateral flow immunoassay, Anal. Chem. 92 (2020) 7226–7231.
[20] E.R. Adams, R. Anand, M.I. Andersson, K. Auckland, J.K. Baillie, E. Barnes, S. Beer, J.I. Bell, T. Berry, S. Bibi, et al., Evaluation of antibody testing for SARS-Cov-2 using ELISA and lateral flow immunoassays, medRxiv (2020) 04.15.20066407.
[21] G. Qiu, Z. Gai, Y. Tao, J. Schmitt, G.A. Kullak-Ublick, J. Wang, Dual-functional plasmonic photothermal biosensors for highly accurate severe acute respiratory syndrome coronavirus 2 detection, ACS Nano 14 (2020) 268–5277.
[22] A. Ahmadivand, B. Gerislioglu, Z. Ramezani, A. Kaushik, P. Manickam, S.A. Ghoreishi, Femtomolar-level detection of SARS-CoV-2 spike proteins using toroidal plasmonic metasensors, arXiv (2020) 2006.08536.
[23] Y. Fang, H. Zhang, J. Xie, M. Lin, L. Ying, P. Pang, W. Ji, Sensitivity of chest CT for COVID-19: comparison to RT-PCR, Radiology 296 (2020) E115–E117.
[24] L. Fabiani, M. Saroglia, G. Galatà, R. De Santis, S. Fillo, V. Luca, G. Faggioni, N. D'Amore, E. Regalbuto, P. Salvatori, et al., Magnetic beads combined with carbon black-based screen-printed electrodes for COVID-19: a reliable and miniaturized electrochemical immunosensor for SARS-CoV-2 detection in saliva, Biosens. Bioelectron. 171 (2020), 112686.
[25] G. Seo, G. Lee, M.J. Kim, S. Baek, M. Choi, K.B. Ku, C. Lee, S. Jun, D. Park, H. G. Kim, et al., Rapid detection of COVID-19 causative virus (SARS-CoV-2) in human nasopharyngeal swab specimens using field-effect transistor based biosensor, ACS Nano 14 (2020) 5135–5142.
[26] R.M. Torrente-Rodríguez, H. Lukas, J. Tu, J. Min, Y. Yang, C. Xu, H.B. Rossiter, W. Gao, SARS-CoV-2 RapidPlex: a graphene-based multiplexed telemedicine platform for rapid and low-cost COVID-19 diagnosis and monitoring, Matter 3 (2020) 1–18.
[27] B.S. Vadlamani, T. Uppal, S.C. Verma, M. Misra, Functionalized TiO_2 nanotube-based electrochemical biosensor for rapid detection of SARS-CoV-2, Sensors 20 (2020) 5871.
[28] H. Zhao, F. Liu, W. Xie, T.C. Zhou, J. OuYang, L. Jin, H. Li, C.Y. Zhao, L. Zhang, J. Wei, et al., Ultrasensitive supersandwich-type electrochemical sensor for SARS-CoV-2 from the infected COVID-19 patients using a smartphone, Sens. Actuators B: Chem. 327 (2021), 128899.
[29] Z. Rahmati, M. Roushani, H. Hosseini, H. Choobin, Electrochemical immunosensor with Cu_2O nanocube coating for detection of SARS-CoV-2 spike protein, Microchim. Acta 188 (2021) 105.
[30] B. Mojsoska, S. Larsen, D.A. Olsen, J.S. Madsen, I. Brandslund, F.A. Alatraktchi, Rapid SARS-CoV-2 detection using electrochemical immunosensor, Sensors 21 (2021) 390.
[31] S. Eissa, M. Zourob, Development of a low-cost cotton-tipped electrochemical immunosensor for the detection of SARS-CoV-2, Anal. Chem. 93 (2021) 1826–1833.
[32] L.M. Kucirka, S.A. Lauer, O. Laeyendecker, D. Boon, J. Lessler, Variation in false-negative rate of reverse transcriptase polymerase chain reaction-based SARS-CoV-2 tests by time since exposure, Ann. Intern. Med. 173 (2020) 262–267.
[33] T. Ai, Z. Yang, H. Hou, C. Zhan, C. Chen, W. Lv, Q. Tao, Z. Sun, L. Xia, Correlation of chest CT and RT-PCR testing for coronavirus disease 2019 (COVID-19) in China: a report of 1014 cases, Radiology 296 (2020) E32–E40.
[34] X.L. Wang, H.P. Yao, X. Xu, P.Y. Zhang, M.M. Zhang, J.B. Shao, Y.Q. Xiao, H. L. Wang, Limits of detection of six approved RT-PCR kits for the novel SARS-coronavirus-2 (SARS-CoV-2), Clin. Chem. 66 (2020) 977–979.
[35] Z. Ye, Y. Zhang, Y. Wang, Z. Huang, B. Song, Chest CT manifestations of new coronavirus disease 2019 (COVID-19): a pictorial review, Eur. Radiol. 30 (2020) (2019) 4381–4389.
[36] M.S. Khan, S.K. Misra, K. Dighe, Z. Wang, A.S. Schwartz-Duval, D. Sar, D. Pan, Electrically-receptive and thermally responsive paper-based sensor chip for rapid detection of bacterial cells, Biosens. Bioelectron. 110 (2018) 132–140.
[37] M.S. Khan, K. Dighe, Z. Wang, I. Srivastava, A.S. Schwartz-Duval, S.K. Misra, D. Pan, Electrochemical-digital immunosensor with enhanced sensitivity for detecting human salivary glucocorticoid hormone, Analyst 144 (2019) 1448–1457.

[38] F. Liu, K.S. Choi, T.J. Park, S.Y. Lee, T.S. Seo, Graphene-based electrochemical biosensor for pathogenic virus detection, Biochip J. 5 (2011) 123–128.
[39] R. Wang, C. Xue, M. Gao, H. Qi, C. Zhang, Ultratrace voltammetric method for the detection of DNA sequence related to human immunodeficiency virus type 1, Microchim. Acta 172 (2011) 291–297.
[40] L.A. Layqah, S. Eissa, An electrochemical immunosensor for the corona virus associated with the Middle East respiratory syndrome using an array of gold nanoparticle-modified carbon electrodes, Microchim. Acta 186 (2019) 224.